Draft version February 10, 2019
Typeset using LaTeX **preprint** style in AASTeX62

The Star-Forming Sequence in a Hierarchical Universe

ChangHoon Hahn,[1,2,3,*] Jeremy L. Tinker,[3] and Andrew R. Wetzel[4,5,6]

[1] *Lawrence Berkeley National Laboratory, 1 Cyclotron Rd, Berkeley CA 94720, USA*
[2] *Berkeley Center for Cosmological Physics, University of California, Berkeley, CA 94720, USA*
[3] *Center for Cosmology and Particle Physics, Department of Physics, New York University, 4 Washington Place, New York, NY 10003*
[4] *TAPIR, California Institute of Technology, Pasadena, CA USA*
[5] *Carnegie Observatories, Pasadena, CA USA*
[6] *Department of Physics, University of California, Davis, CA USA*

ABSTRACT

sentence on the questions of SF galaxies. Star-forming galaxies are observed to have a tight relationship between their star formation rates and stellar masses. This so-called "star-forming sequence" (SFS) characterizes both the star formation histories and stellar mass growth of star-forming galaxies. Meanwhile, observed constraints on the stellar-to-halo mass relation (SHMR) connect the stellar mass growth of galaxies to their host halo halo accretion history. Combining these observed trends with a high-resolution cosmological N-body simulation, we present a model that tracks the star formation, stellar mass, and host halo accretion histories of star-forming central galaxies over $z < 1$. By comparing this model to the observed stellar mass function and SFS of central galaxies in the SDSS Data Release 7, we find that star formation variability on timescales $\lesssim 0.5\,\mathrm{Gyr}$ is *necessary* to produce tighter scatter in the SHMR, $\sigma_{\log M_*}$, at $M_h{=}10^{12} M_\odot$ comparable to observations. However, to conservatively reproduce the observed $\sigma_{\log M_*}{\sim}0.2\,\mathrm{dex}$, the star formation histories must also correlate strongly with halo accretion history with a correlation coefficient $r > 0.5$ — *i.e.* exhibit strong assembly bias. The timescale of star formation variability and the correlation between star formation and halo accretion history we infer, provide key constraints on the star formation history and the evolution of star-forming central galaxies.

Keywords: methods: numerical – galaxies: clusters: general – galaxies: groups: general – galaxies: evolution – galaxies: haloes – galaxies: star formation – cosmology: observations.

1. INTRODUCTION

Observations from surveys such as the Sloan Digital Sky Survey (SDSS; **?**), Cosmic Evolution Survey (COSMOS; Scoville et al. 2007), and the PRIsm MUlti-object Survey (PRIMUS; Coil et al. 2011; Cool et al. 2013) have provided statistically meaningful samples of galaxies, which have been

* hahn.changhoon@gmail.com

critical for establishing the global trends of galaxies in the local universe. Broadly speaking, galaxies fall into two categories: quiescent and star-forming galaxies. Quiescent galaxies have little to no star formation, are red in color, and have ellipitical morphologies. Meanwhile, star-forming galaxies have significant star formation, are blue in color, and have disk-like morphologies (**??**Baldry et al. 2006; **?**; Moustakas et al. 2013; see Blanton & Moustakas 2009 and references therein).

Star-forming galaxies, furthermore, are found on the so-called "star-forming sequence" (hereafter SFS), a tight relationship between their star formation rates (SFR) and stellar masses (Noeske et al. 2007; Daddi et al. 2007; Salim et al. 2007; Speagle et al. 2014; Lee et al. 2015, see also Figure 1). This sequence, which is observed out to $z > 2$ (Wang et al. 2013; **?**; **?**), plays a crucial role in characterizing galaxy evolution over the past $\sim$10 Gyr. The significant fraction of star-forming galaxies that quench their star formation and migrate off of the SFS reflects the significant growth in the fraction of quiescent galaxies (**???**Moustakas et al. 2013). Meanwhile, the decline of star formation in the entire SFS (Lee et al. 2015; **?**) over time reflects the decline in overall cosmic star formation (**???**). The SFS and its evolution also connects star formation history and stellar mass growth of star-forming galaxies.

CH: some blanket statements about connection between galaxy-halo connection For instance, the stellar-to-halo mass relation (SHMR) is constrained from **papers that look at SHMR or sigma of that from high redsihft** (Mandelbaum et al. 2006; Conroy et al. 2007; More et al. 2011; Leauthaud et al. 2012; Tinker et al. 2013; Velander et al. 2014; Han et al. 2015; Zu & Mandelbaum 2015; Gu et al. 2016) Constraints on the SHMR at $z \sim 1$ from observations find Remarkably, at $z \sim 0$, observational constraints find little evolution in the scatter in the SHMR. These observational constraints suggest that stellar mass growth of galaxies are closely linked to the hierarchical growth of their host dark matter halos.

Despite our understanding of the evolving galaxy population in a hierarchical unvierse, we face a number of challenges when it comes to understanding their detailed star formation histories (SFH). For instance, SFHs at lookback times longer than 200 Myr do not contribute to SFR indicators such as $H\alpha$ or FUV fluxes. Measuring SFHs from fitting photometry or spectroscopy typically assume a specific functional form of the SFH, such as exponentially declining or lognormal, that do not include short timescale variability (*e.g.* Wilkinson et al. 2017; Carnall et al. 2018). Even methods that recover non-parametric SFHs from high signal-to-noise observations can only retrieve SFHs in coarse temporal resolutions (*e.g.* Tojeiro et al. 2009; Leja et al. 2018). While simulations provide another means for understanding SFHs, are also subject to their specific time and mass resolutions that suppress the variability of their star formation, especially in analytic models, semi-analytic models, and large-volume cosmological simulations (**?**). These challenges make difficult to constrain certain things like the timescale of star formation variability.

CH: paragraph on assembly bias and how we've look at it w.r.t. quenching and stuff but it's still unclear at a sfh level. Also talk about previous empirical models that do this but emphasize that they do not focus on the timescale. Something along the lines of Along with the fraction of random variations in galaxy SFRs, the random variations' timescales also need parameterization. Longer-timescale random variations can arise from galactic feed- back interacting with the circumgalactic

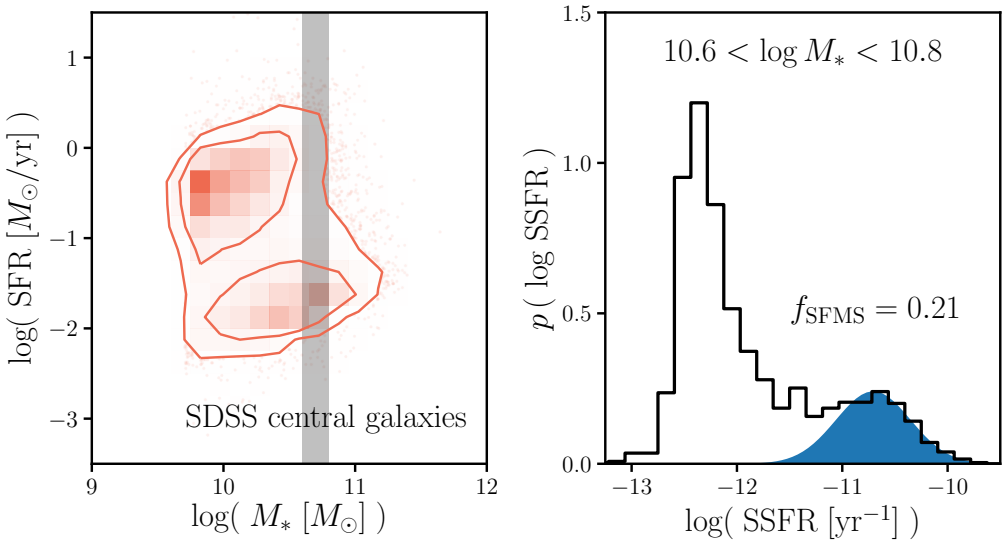

Figure 1. The SFR–M_* relation of the central galaxies in SDSS DR7 mark the bimodal distribution of the star-forming and quiescent populations (left panel). *Star-forming centrals, based on the correlation between their SFR and M_*, lie on the so-called "star-forming sequence"*. On the right, we present the SSFR distribution, $p(\log \mathrm{SSFR})$, of SDSS centrals with $10.6 < \log M_* < 10.8$. Based on the SFS component from the Hahn et al. (2018) GMM fit to the SFR–M_* relation (shaded in blue), galaxies in the SFS account for $f_{\rm SFS} = 0.21$ of the centrals in the stellar mass bin.

medium and larger-scale environment. At the same time, short-timescale (10 100 Myr) variations occur due to internal processes affecting local galac- tic cold gas.

CH: emphasize how we're focusing on the SFH In this paper, we take advantage of this connection between SFH and the underlying dark matter to constrain the SFH of star-forming central galaxies. We focus on central galaxies since the SFHs of satellites are likely influenced by environmentally-driven external mechanisms such as ram pressure stripping (Gunn & Gott 1972; Bekki 2009), strangulation (Larson et al. 1980; Balogh et al. 2000), or harassment (Moore et al. 1998). Moreover, centrals constitute the majority of massive galaxies ($M_* > 10^{9.5} M_\odot$) at $z \sim 0$ (Wetzel et al. 2013). Using a similar approach as Wetzel et al. (2013); **?**, we present a model that combines a high resolution cosmological N-body simulation with observed evolutionary trends of the SFS. Our model statistically tracks the star formation, stellar mass, and host halo mass histories of star-forming central galaxies over $z \sim 1$ to 0. By comparing predictions of this empirical model to observations, we constrain the timescale of star formation variability and also the correlation between SFH and host halo history. **sentence on implication**

In Section 2 we describe the $z \approx 0$ central galaxy sample that we construct from SDSS Data Release 7. Then in Section 3, we describe the N-body simulation and how we evolve the SFR and stellar masses of the star-forming central galaxies in our model. We compare predictions from our model to observations and present the resulting constraints in Section 4. Finally, we conclude and summarize the results in Section 5.

2. CENTRAL GALAXIES OF SDSS DR7

We construct our galaxy sample following the sample selection of Tinker et al. (2011). We select a volume-limited sample of galaxies at $z \approx 0.04$ with $M_r - 5\log(h) < -18$ and complete above $M_* > 10^{9.4} M_\odot$ from the NYU Value-Added Galaxy Catalog (VAGC; Blanton et al. 2005) of the Sloan Digital Sky Survey Data Release 7 (SDSS DR7; Abazajian et al. 2009). The stellar masses of these galaxies are estimated using the `kcorrect` code (Blanton & Roweis 2007) assuming a Chabrier (2003) initial mass function. For their specific star formation rates (SSFR) we use measurements from the current release of the MPA-JHU spectral reductions[1] (Brinchmann et al. 2004). Generally, SSFR $> 10^{-11}\mathrm{yr}^{-1}$ are derived from Hα emission, $10^{-11} >$ SSFR $> 10^{-12}\mathrm{yr}^{-1}$ are derived from a combination of emission lines, and SSFR $< 10^{-12}\mathrm{yr}^{-1}$ are based on D_n4000 (see discussion in Wetzel et al. 2013). We emphasize that SSFR $< 10^{-12}\mathrm{yr}^{-1}$ should only be considered upper limits to the actual galaxy SSFR (Salim et al. 2007).

From this galaxy sample, we identify central galaxies using the Tinker et al. (2011) group finder, a halo-based algorithm that uses the abundance matching ansatz to iteratively assign halo masses to groups. It initially assigns a tentative halo mass to each galaxy by matching their abundances. Then starting with the most massive galaxy, nearby lower mass galaxies are assigned a probability of being a satellite. Once all the galaxies are assigned to a group, the halo masses of the central galaxies are updated by abundance matching with the total stellar mass in the groups. This entire process is repeated until convergence. Every group contains one central galaxy, which by definition is the most massive, and a group can contain zero, one, or many satellites. As with any group finder, galaxies are misassigned due to projection effects and redshift space distortions. Our central galaxy sample has a purity of ∼90% and completeness of ∼95% (**?**) Moreover, as illustrated in Campbell et al. (2015), the Tinker et al. (2011) group finder robustly identifies red and blue centrals as a function of stellar mass, which is highly relevant to our analysis. We present the SFR–M_* relation of the SDSS DR7 central galaxies, described above, in the left panel of Figure 1. The contours of the relation clearly illustrate the bimodality in the galaxy sample with the star-forming centrals lying on the so-call "star-forming sequence" (SFS).

3. MODEL: SIMULATED CENTRAL GALAXIES

We're interesting in constructing a model that tracks central galaxies and their star formation within the heirarchical growth of their host halos. This requires a cosmological N-body simulation that accounts for the complex dynamical processes that govern the host halos of galaxies. In this paper we use the high resolution N-body simulation from Wetzel et al. (2013) generated using the White (2002) `TreePM` code with flat ΛCDM cosmology ($\Omega_m = 0.274, \Omega_b = 0.0457, h = 0.7, n = 0.95$, and $\sigma_8 = 0.8$). From initial conditions at $z = 150$, generated from second-order Lagrangian Perturbation Theory, 2048^3 particles with mass of $1.98 \times 10^8\, M_\odot$ are evolved in a $250\,\mathrm{Mpc}/h$ box with a Plummer equivalent smoothing of $2.5\,\mathrm{kpc}/h$ (Wetzel et al. 2013, 2014). 'Host halos' are then identified using the Friends-of-Friends algorithm (FoF; Davis et al. 1985) with linking length of b=0.168 times the

[1] http://wwwmpa.mpa-garching.mpg.de/SDSS/DR7/

mean inter-partcile spacing. Within these host halos, Wetzel et al. (2013) identifies 'subhalos' as overdensities in phase space through a six-dimensional FoF algorithm (FoF6D; White et al. 2010). The host halos and subhalos are then tracked across the simulation outputs from $z = 10$ to 0 to build merger trees (Wetzel et al. 2009; Wetzel & White 2010). The most massive subhalos in newly-formed host halos at a given simulation output are defined as the 'central' subhalo. A central subhalo retains its 'central' definition until it falls into a more massive host halo, at which point it becomes a 'satellite' subhalo.

Throughout its 45 snapshot outs, `TreePM` simulation tracks the evolution of subhalos back to $z \sim 10$. We restrict ourselves to 15 snapshots from $z = 1.08$ to 0.05, where we have the most statistically meaningful observations. Furthermore, since we're interested in centrals we only keep subhalos that are classified as centrals throughout the redshift range. This criterion removes "black splash" or "ejected" satellite galaxies (*e.g.* Mamon et al. 2004; Wetzel et al. 2014) misclassified as centrals. Next, we describe how we select and initialize the star-forming central galaxies from the central subhalos of the `TreePM` simulation in our model.

3.1. *Selecting Star-Forming Centrals*

To construct a model that tracks the SFR and stellar mass evolution of star-forming central galaxies, we first need to select them from the central galaxies/subhalos in the `TreePM` simulation. Since we want our model to reproduce observations, our selection is based on $f^{\rm cen}_{\rm SFS}(M_*)$, the fraction of central galaxies within the SFS measured from the SDSS DR7 VAGC (Section 2). Below, we describe how we derive $f^{\rm cen}_{\rm SFS}(M_*)$ and use it to select star-forming central galaxies in our model. Afterwards we describe how we initialize the SFRs and M_* of these galaxies.

Often in the literature, an empirical color-color or SFR–M_* cut that separates the two main modes (red/blue or star-forming/quiescent) in the distribution is chosen to classify galaxies (*e.g.* Baldry et al. 2006; Blanton & Moustakas 2009; Drory et al. 2009; Peng et al. 2010; Moustakas et al. 2013; Hahn et al. 2015). The red/quiescent or blue/star-forming fractions derived from this sort of classification, by construction, depend on the choice of cut and neglect galaxy subpopulations such as transitioning galaxies *i.e.* galaxies in the "green valley". Instead, for our $f^{\rm cen}_{\rm SFS}(M_*)$, we use the SFS identified from the Hahn et al. (2018) method. Hahn et al. (2018) uses Gaussian Mixture Models and the Bayesian Information Criteria in order to fit the SFR–M_* relation of a galaxy population and identify its SFS. This data-driven approach relaxes many of the assumptions and hard cuts that go into other methods. Furthermore, Hahn et al. (2018) demonstrate its method can be flexibly applied to a wide range of SFRs and M_*s and for multiple simulations. The weight of the SFS GMM component from the method provides an estimate of $f^{\rm cen}_{\rm SFS}$. In the right panel of Figure 1, we present the SSFR distribution, $p(\log \mathrm{SSFR})$, of the SDSS DR7 central galaxies within $10.6 < \log M_* < 10.8$ with the SFS GMM component shaded in blue. The SFS constitutes $f^{\rm cen}_{\rm SFS} = 0.21$ of the SDSS central galaxies in this stellar mass bin. Using the $f^{\rm cen}_{\rm SFS}$ estimates, we fit $f^{\rm cen}_{\rm SFS}$ as a linear function of $\log M_*$ similar to Wetzel et al. (2013); Hahn et al. (2017a):

$$f^{\rm cen}_{\rm SFS,bestfit}(M_*) = -0.627\,(\log\, M_* - 10.5) + 0.354. \quad (1)$$

We note that this is in good agreement with the $f^{\rm cen}_{\rm Q}(M_*; z \sim 0)$ fit from Hahn et al. (2017a).

For each central subhalo in our simulation, we assign a probability of it being on the SFS, using Eq. 1 with M_* at $z \sim 0$ assigned through subhalo abundance matching (SHAM) to $M_{\rm peak}$, the maxmum host halo mass that it ever had as a central subhalo (Conroy et al. 2006; Vale & Ostriker 2006; Yang et al. 2009; Wetzel et al. 2012; Leja et al. 2013; Wetzel et al. 2013, 2014; Hahn et al. 2017a). SHAM, in its simplest form, assumes a one-to-one mapping between subhalo $M_{\rm peak}$ and galaxy stellar mass, M_*, that preserves rank order: $n(>M_{\rm peak}) > n(>M_*)$. In practice, we apply a 0.2 dex log-normal scatter in M_* at fixed $M_{\rm peak}$ based on the observed SHMR. For $n(>M_*)$, we use observed stellar mass function (SMF) from Li & White (2009), which is based on the same SDSS NYU-VAGC sample as our group catalog. Based on the probabilities from Eq. 1 and SHAM M_*, we randomly identify centrals from our simulation as SF at $z \sim 0$. Tinker et al. (2017, 2018b) found that quenching is independent of halo growth rate and therefore we randomly select SF subhalos. In our model, we assume that once a SF galaxy quenches its star formation, it remains quiescent. Without any quiescent galaxies rejuvenating their star formation, galaxies on the SFS at $z \sim 0$ are also on the SFS at $z > 0$. Using this assumption the SF centrals we select at $z \sim 0$ are also on the SFS at the intial redshift of our model: $z \sim 1$.

We next initialize the SF centrals at $z \sim 1$ using the observed SFR-M_* relation of the SFS with M_* assigned using SHAM with a SMF interpolated between the Li & White (2009) SMF and the SMF from Marchesini et al. (2009) at $z = 1.6$. We choose the Marchesini et al. (2009) SMF, among others, because it produces interpolated SMFs that monotonically increase at $z < 1$. As noted in Hahn et al. (2017a), at $z \approx 1$, the SMF interpolated between the Li & White (2009) and Marchesini et al. (2009) SMFs is consistent with more recent measurements from Muzzin et al. (2013) and Ilbert et al. (2013). Observations in the literature at $z \sim 1$, however, not only use galaxy properties derived differently from the SDSS VAGC but they also find SFS with significant discrepancies from one another. Speagle et al. (2014) compiles the SFR-M_* relation of the SFS from 25 studies in the literature, each with different methods of deriving galaxy properties. Even *after* their calibration, for a fixed $M_* = 10^{10.5}\,M_\odot$, the SFRs of the SFSs at $z \sim 1$ vary by more than a factor of 2 (see Figure 2 of Speagle et al. 2014). With little consensus on the SFS at $z \sim 1$, and consequently its redshift evolution, we flexibly parameterize the SFS SFR, $\log {\rm SFR}_{\rm SFS}(M_*, z)$, with free parameters $m_{M_*}^{\rm low}$, $m_{M_*}^{\rm high}$, and m_z. These parameters characterize the stellar mass dependence of the SFS below and above $10^{10} M_\odot$ and its redshift dependence, respectively.

We parameterize the $\log {\rm SFR}$ of the SFS as,

$$\log {\rm SFR}(M_*, z) = \begin{cases} m_{M_*}^{\rm low}\,(\log M_* - 10.) & \text{for } M_* < 10^{10} M_\odot \\ m_{M_*}^{\rm high}\,(\log M_* - 10.) & \text{for } M_* \geq 10^{10} M_\odot. \end{cases} + m_z (z - 0.05) - 0.19. \qquad (2)$$

We assign SFRs to our SF centrals at $z \sim 1$ by sampling a log-normal distribution centered about $\log {\rm SFR}_{\rm MS}(M_*, z = 1)$ with a constant scatter of 0.3 dex, motivated from observations (Daddi et al. 2007; Noeske et al. 2007; Magdis et al. 2012; Whitaker et al. 2012). Later when comparing to observations, we choose conservative priors for the parameters $m_{M_*}^{\rm low}$, $m_{M_*}^{\rm high}$ and m_z that encompass the best-fit SFS from Speagle et al. (2014) and measurements from Moustakas et al. (2013) and Lee et al. (2015). With our SF centrals initalized at $z \sim 1$, next, we describe how we evolve their SFR and M_*.

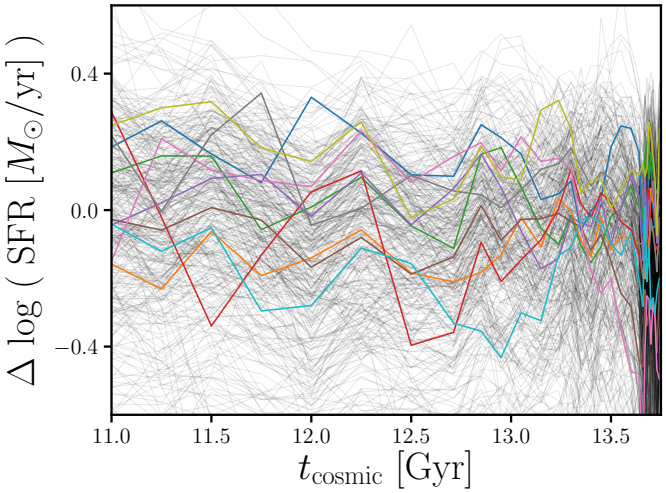

Figure 2. Galaxies in the Illustris simulation have SFHs that evolve along the SFS, with their SFRs stochastically fluctuating about the $\log \mathrm{SFR}$ of the SFS. We highlight $\Delta \log \mathrm{SFR}$, SFR with respect to $\log \mathrm{SFR}_{\mathrm{SFS}}$ (Eq. 3), for a handful of galaxies with $10^{10.5} < M_* < 10^{10.6} M_\odot$ at $z \sim 0$. We calculate $\Delta \log \mathrm{SFR}$ with $\log \mathrm{SFR}_{\mathrm{SFS}}$ identified using the Hahn et al. (2018) method, same as in Section 3.1. The implementation of SFR variability in the SFHs of star-forming centrals in our model (Section 3.2) is motivated by the SFHs of Illustris galaxies above.

3.2. *Evolving along the Star Formation Sequence*

The tight correlation between the SFRs and stellar masses of star-forming galaxies on the SFS has been observed spanning over four orders of magnitude in stellar mass, with a roughly constant scatter of $\sim$0.3 dex, and out to $z > 2$ (*e.g.* Noeske et al. 2007; Daddi et al. 2007; Elbaz et al. 2007; Salim et al. 2007; Santini et al. 2009; Karim et al. 2011; Whitaker et al. 2012; Moustakas et al. 2013; Lee et al. 2015; see also references in Speagle et al. 2014). This correlation is also predicted by modern galaxy formation models (Somerville & Davé 2015, see Hahn et al. 2018 and references therein). The SFS naturally presents itself as an anchoring relationship to characterize the star formation and M_* growth histories of SF galaxies throughout $z < 1$. More specifically, *we characterize the SFH of each star-forming central with respect to the* $\log \mathrm{SFR}$ *of the SFS* (Eq. 2):

$$\log \mathrm{SFR}_i(M_*, t) = \log \mathrm{SFR}_{\mathrm{SFS}}(M_*, t) + \Delta \log \mathrm{SFR}_i(t). \tag{3}$$

Since SFHs determine the M_* growth of galaxies, in this prescription, $\Delta \log \mathrm{SFR}_i(t)$ dictates the SFH and M_* evolution a star-forming central. Next, we describe our prescription for $\Delta \log \mathrm{SFR}$.

One simple prescription for $\Delta \log \mathrm{SFR}(t)$ would be to keep $\Delta \log \mathrm{SFR}$ fixed throughout $z < 1$ to the offsets from the $\log \mathrm{SFR}_{\mathrm{SFS}}$ in the initial SFRs of our SF centrals at $z \sim 1$ similar to simple analytic models such as Mitra et al. (2015). Galaxies with higher than average initial SFRs continue evolving above the average SFS, while SF centrals with lower than average initial SFRs continue evolving below the average SFS. In addition to not being able to reproduce observations, which we later demonstrate, we also do not find such SFHs in SF galaxies of hydrodynamic simulations such as Illustris (Vogelsberger et al. 2014; Genel et al. 2014). In Figure 2, we plot $\Delta \log \mathrm{SFR}_i$ of star-forming

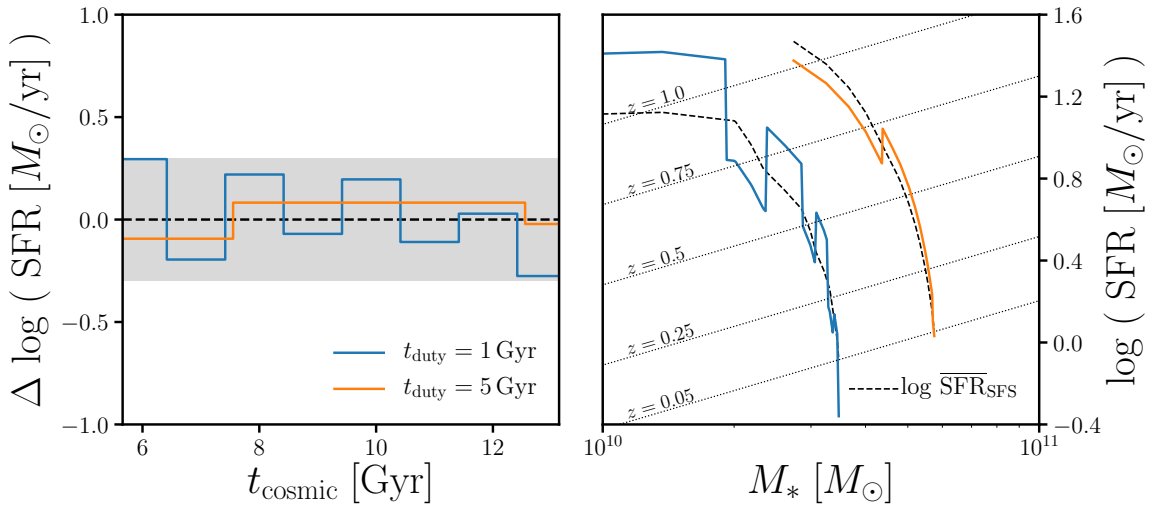

Figure 3. We incorporate star formation variability in our model using a "star formation duty cycle" where the SFRs of SF centrals fluctuate about the $\log \mathrm{SFR}_{\mathrm{SFS}}$ on some timescale t_{duty}. In our fiducial prescription, we randomly sample $\Delta \log \mathrm{SFR}$ from a log-normal distribution with 0.3 dex scatter at each timestep. We illustrate $\Delta \log \mathrm{SFR}_i(t)$ of two SF centrals with star formation duty cycles on $t_{\mathrm{duty}} = 1$ Gyr (blue) and 5 Gyr (orange) timescales in the left panel. $\Delta \log \mathrm{SFR}(t)$ determines the SFH and hence the M_* growth of the SF central galaxies (Eq. 4). On the right, we illustrate the SFR and M_* evolutions of the corresponding SF centrals. For reference, we include $\log \mathrm{SFR}_{\mathrm{SFS}}(M_{*,i}(t), t)$ that the galaxies' SFR and M_* evolve along (black solid). We also include $\log \mathrm{SFR}_{\mathrm{SFS}}(M_*)$ at various redshifts between $z = 1$ to 0.05 (dotted lines). *The star-forming centrals in our model evolve their SFRs and M_* along the SFS with their SFRs fluctuate about* $\log \mathrm{SFR}_{\mathrm{SFS}}$.

galaxies in the Illustris simulation as a function of cosmic time. These galaxies have stellar masses within $10^{10.5} - 10^{10.6} M_\odot$ at $z = 0$. At each simulation output, we calculate $\Delta \log \mathrm{SFR}$ using Eq. 3 with $\log \mathrm{SFR}_{\mathrm{SFS}}$ derived from the SFS identified using the same Hahn et al. (2018) method as in Section 3.1. As the highlighted $\Delta \log \mathrm{SFR}_i$ illustrate, star-forming galaxies in Illustris evolve along the SFS, with their SFRs fluctuating about $\log \mathrm{SFR}_{\mathrm{SFS}}$.

Motivated by the SFHs of Illustris SF galaxies, we introduce variability to the SFHs of our SF centrals in the form of a "*star formation duty cycle*". Within the Eq. 3 SFH, we parameterize $\Delta \log \mathrm{SFR}_i$ to fluctuate about the $\log \mathrm{SFR}_{\mathrm{SFS}}$ on timescale, t_{duty}, with amplitude sampled to reproduce the observed log-normal distribution with 0.3 dex scatter at every timestep. For our fiducial star formation duty cycle prescription, we randomly sample $\Delta \log \mathrm{SFR}_i$ from a log-normal distribution with $\sigma = 0.3$ dex. We illustrate $\Delta \log \mathrm{SFR}_i(t)$ of SF centrals with our star formation duty cycle prescription on $t_{\mathrm{duty}} = 1$ Gyr (blue) and 5 Gyr (orange) timescales in the left panel of Figure 3. The shaded region represents the observed 0.3 dex 1σ scatter of $\log \mathrm{SFR}$ in the SFS. This $\Delta \log \mathrm{SFR}$ prescription by construction reproduces the observed log-normal SFR distribution of the SFS at any point in the model. Although, we do not expect this simplified prescription to reflect the individual SFHs of SF centrals, we seek to statistically capture the stochasticity from gas accretion, star-bursts, and feedback mechanisms for the entire SF population. Measuring t_{duty} in the duty cycle parame-

terization provides us with an estimate of the timescale of such star formation variabilities and thus provide additional useful constraints on the physics of galaxy formation.

Using our fiducial SFH prescription, we evolve both the SFR and M_* of our SF centrals along the SFS. Based on Eq. 3, the SFRs of our SF centrals are functions of M_*. Meanwhile, M_* is the integral of the SFR over time:

$$M_*(t) = f_{\rm retain} \int_{t_0}^{t} \mathrm{SFR(M_*, t)\, dt} + M_0. \tag{4}$$

t_0 and M_0 are the initial cosmic time and stellar mass at $z \sim 1$, respectively. $f_{\rm retain}$ here is the fraction of stellar mass that is retained after supernovae and stellar winds; we use $f_{\rm retain} = 0.6$ (Wetzel et al. 2013). We can now evolve the SFR and M_* of our star-forming centrals until the final $z = 0.05$ snapshot by solving the differential equation of Eqs. 3 and 4. On the right panel of Figure 3, we present the SFR and M_* evolutions of two SF centrals with $t_{\rm duty} = 1$ Gyr (blue) and 5 Gyr (orange), same as the left panel. For reference, we include the mean $\log \mathrm{SFR}$ of the SFS that the galaxies' SFR and M_* evolve along, $\log \mathrm{SFR_{SFS}}(M_{*,i}(t), t)$ (black solid). We also include $\log \mathrm{SFR_{SFS}}(M_*)$ (dotted lines) at various redshifts between $z = 1$ to 0.05. Based on the SFH prescription in our model, star-forming centrals evolve their SFRs and M_* along the SFS with their SFRs fluctuate about $\log \mathrm{SFR_{SFS}}$.

With the evolved SFRs and M_* of SF centrals, we can compare our model to observed galaxy population scatistics such as the quiescent fraction and SMF to constrain its free parameters. Our model, run with these inferred parameters, then reproduces observations of galaxy properties and has host halo properties from the `TreePM` N-body simulation. This allows us to compare our models to observations of the galaxy-halo connection such as the SHMR. In the following section, we present this comparison and the constraints we derive on the role and timescale of star formation variability in SF central galaxies.

4. RESULTS

Our model takes `TreePM` central subhalos and tracks their SFR and M_* evolution using a flexible parameterization of the SFS and SFHs that incorporate variability through a star formation duty cycle. At $z = 0.05$, its final timestep, our model predicts properties such as SFR, M_*, and host halo mass, M_h, of central galaxies it classifies as star-forming. We now use these resulting properties to compare our model to observations and constrain its free parameters— the SFS parameters of Eq. 2. Since the focus of our model and this paper is SF centrals, the main observable we use is the SMF of SF centrals in SDSS, which we estimate as

$$\Phi^{\rm SDSS}_{\rm SF,cen} = f^{\rm cen}_{\rm SFS} \times f_{\rm cen} \times \Phi^{\rm Li\&White(2009)}. \tag{5}$$

$f^{\rm cen}_{\rm SFS}$ is the fraction of central galaxies on the SFS, which we fit in Eq. 1. $f_{\rm cen}$ is the central galaxy fraction from Wetzel et al. (2013) and $\Phi^{\rm Li\&White(2009)}$ is the SMF of the SDSS from Li & White (2009). If our model reproduces the observed $\Phi^{\rm SDSS}_{\rm SF,cen}$, by construction it reproduces the observed quiescent fraction.

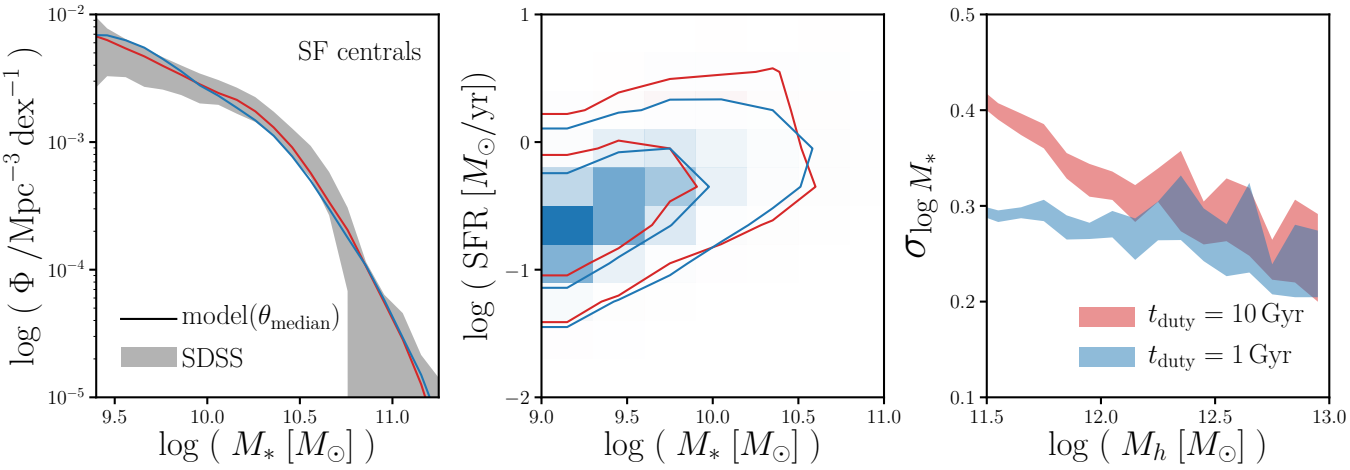

Figure 4. Our models with different star formation duty cycle timescales (blue: $t_{\rm duty}$=1 Gyr; red: $t_{\rm duty}$=10 Gyr) run with median values of their ABC posterior distribution have SMFs and SFSs consistent with observations (left and middle). *They however produce significantly different scatter in* log M_* *at fixed* log $M_{\rm halo}$ *— scatter in the SHMR (right).* By comparing the scatter in SHMR of our models to observational constraints on the SHMR, we constrain the timescale of the star formation duty cycle and thereby the SFHs of star forming galaxies.

For the comparison between our model to observation, we use the parameter estimation framework of Approximate Bayesian Computation (ABC). ABC has the advantage over standard approaches to parameter inference in that it does not require evaluating the likelihood. It relies only on a simulation of the observed data and a distance metric to quantify the "closeness" between the observed data and simulation. Many variations of ABC has been used in astronomy and cosmology (*e.g.* Cameron & Pettitt 2012; Weyant et al. 2013; Ishida et al. 2015; Alsing et al. 2018). We use ABC in conjunction with the efficient Population Monte Carlo (PMC) importance sampling as in (Hahn et al. 2017a,b). For initial sampling of our ABC particles, *i.e.* the priors of our parameters $m_{M_*}^{\rm low}$, $m_{M_*}^{\rm high}$, and m_z, we use uniform distributions over the ranges $[0.0, 0.8]$, $[0.0, 0.8]$, and $[0.5, 2.]$, respectively. As we mention earlier in Section 3.1, the range of the prior were conservatively chosen to encompass the best-fit SFS from Speagle et al. (2014) and measurements from Moustakas et al. (2013) and Lee et al. (2015) at $z \sim 1$. Finally, for our distance metric we use the following distance between the SMF of the star-forming centrals in our model to the observed $\Phi_{\rm SF,cen}^{\rm SDSS}$:

$$\rho_\Phi = \sum_M \left(\frac{\Phi^{\rm sim} - \Phi_{\rm SF,cen}^{\rm SDSS}}{\sigma'_\Phi} \right)^2 . \tag{6}$$

$\Phi^{\rm sim}(M)$ above is the SMF of the SF centrals in our model and $\sigma'_\Phi(M)$ is the uncertainty of $\Phi_{\rm SF,cen}^{\rm SDSS}$, which we derive by scaling the Li & White (2009) uncertainty of $\Phi^{\rm SDSS}$ derived from mock catalogs. For the rest of our ABC-PMC implementation, we strictly follow the implementation of Hahn et al. (2017b) and Hahn et al. (2017a). We refer reader to those papers for further details.

4.1. *Timescale of the Star Formation Duty Cycle*

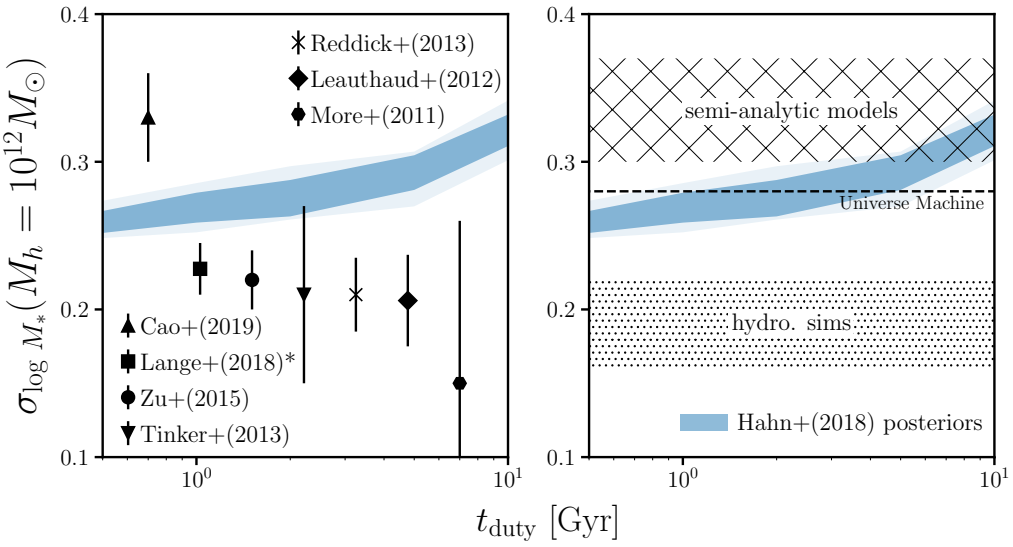

Figure 5. With shorter star formation duty cycle timescales, $t_{\rm duty}$, our model predicts smaller scatter in $\log M_*$ at $M_h = 10^{12} M_\odot$ — $\sigma_{\log M_*}$ (blue). The dark and light blue shaded regions represent the 68% and 95% confidence intervals of $\sigma_{\log M_*}$ predicted from the ABC posteriors of our model with $t_{\rm duty} = 0.5, 1, 2, 5,$ and 10 Gyr. For $t_{\rm duty} = 10$ to 0.5 Gyr, $\sigma_{\log M_*}$ ranges from **CH:** $0.32^{+0.019}_{-0.021}$ to $0.26^{+0.010}_{-0.012}$. In the left panel, we include for comparison observational $\sigma_{\log M_*}$ constraints from Yang et al. (2009); More et al. (2011); Leauthaud et al. (2012); Tinker et al. (2013); Zu & Mandelbaum (2015) and Cao et al. (in preparation) (see Section 4.1). We also include a constrant from Lange et al. (2018); although this constrain is on the scatter in $\log L$ at $M_h = 10^{12} M_\odot$. In the right panel, we include compiled predictions from hydrodyanmical simulations (dotted region), semi-analytic models (hatched), and the UniverseMachine (Behroozi et al. 2018, dashed). Although there is significant tension among the observed constraints, they favor our model with star formation varability on shorter timescales. Meanwhile, even on the shortest timescales we consider, our model does not produce the low $\sigma_{\log M_*} \sim 0.2$ dex predicted by hydrodynamic simulations.

We present the SMFs (left), SFSs (center), and the scatter in $\log M_*$ at a given $\log M_h$, $\sigma_{\log M_*}$, (right) of our model run using SFHs with two different duty cycle timescales, $t_{\rm duty} = 10$ Gyr (red) and 1 Gyr (blue), in Figure 4. For each $t_{\rm duty}$, we evaluate our model at the median parameter values of the respective posterior distributions derived using ABC. For both $t_{\rm duty}$, our model successfully produces SMFs, $\Phi^{\rm SDSS}_{\rm SF,cen}$, and SFSs consistent with observations, as expected (left and center panels). Despite their consistency with observations, however, different $t_{\rm duty}$ of the models predict significantly different $\sigma_{\log M_*}$, particularly below $M_h < 10^{12.5} M_\odot$. We further illustrate the sensitivity of $\sigma_{\log M_*}$ of our model to $t_{\rm duty}$ in Figure 5, where we present $\sigma_{\log M_*}$ at fixed halo mass $M_h = 10^{12} M_\odot$ for our model with $t_{\rm duty} = 0.5, 1, 2, 5,$ and 10 Gyr. As in Figure 4, $\sigma_{\log M_*}$ at each $t_{\rm duty}$ is predicted from our model with parameters from the corresponding ABC posterior distribution. The dark and light blue shaded regions represents the 68% and 95% confidence intervals. For $t_{\rm duty}$ ranging from 10 to 0.5 Gyr, $\sigma_{\log M_*}$ ranges from **CH:** $0.32^{+0.019}_{-0.021}$ to $0.26^{+0.010}_{-0.012}$ — a shorter star formation duty cycle timescale produces significantly smaller scatter in the SHMR. Hence, *observational constraints on the SHMR can be used to constrain the timescale of star formation variability and SFH of SF central galaxies.*

On the left panel of Figure 5, we compare $\sigma_{\log M_*}$ predicted from our model to observational constraints in the literature. These constraints are mainly derived from fitting some sort of halo occupation based models to observations of galaxy clustering, SMF, satellite kinematics, or galaxy-galaxy weak lensing. In Figure 5, we include $\sigma_{\log M_*}$ constraints from More et al. (2011); Leauthaud et al. (2012); Reddick et al. (2013); Tinker et al. (2013); Zu & Mandelbaum (2015) and Cao et al. (in preparation). More et al. (2011), Reddick et al. (2013), and Zu & Mandelbaum (2015) fit SDSS DR7 measurements of satellite kinematics, projected galaxy clustering and conditional stellar mass function, and, galaxy clustering and galaxy-galaxy lensing, repsectively. Meanwhile, Leauthaud et al. (2012); Tinker et al. (2013) use COSMOS to fit the SMF, galaxy clustering, and galaxy-galaxy lensing. Finally, Cao et al. (in preparation) fit the kurtosis of the line-of-sight pairwise velocity dispersion between central galaxies and all neighboring galaxies to constrain the scatter in SHMR at low halo masses. We note that Leauthaud et al. (2012); Reddick et al. (2013); Zu & Mandelbaum (2015) measure $\sigma_{\log M_*}$ for all central galaxies, not only star-forming. Both More et al. (2011); Tinker et al. (2013), however, find a $< 1\sigma$ difference in $\sigma_{\log M_*}$ between SF and quiescent centrals, so we include these constraints in our comparison. We also include the Lange et al. (2018) constraint from fitting color-dependent conditional luminosity function and radial profile of satellite galaxies of SDSS DR7. We note that this constraint is on the scatter in luminosity, $\log L$, not $\log M_*$ at a given M_h.

Aside from Cao et al. (in preparation), the $\sigma_{\log M_*}$ constraints in the literature are consistent: $\sigma_{\log M_*} \sim 0.2$ dex. However, it's important to note that most of these constraints are derived using halo models that fix $\sigma_{\log M_*}$, independent of M_h. As constraining power comes from a wide range of halo masses, such analyses are not ideal for measuring $\sigma_{\log M_*}$ at a specific $M_h \sim 10^{12} M_\odot$. On the other hand, Reddick et al. (2013) constrain $\sigma_{\log M_*}$ for different bins of M_h over the range $10^{12} - 10^{14} M_\odot$ and find little M_h dependence in $\sigma_{\log M_*}$. Their constraints, however, mainly come from the conditional stellar mass function and therefore relies on the accuracy of the Tinker et al. (2011) group finder in identifying halo masses. The constraint from Lange et al. (2018) is also derived from a halo model with M_h dependence. However, as mentioned above, they constrain $\sigma_{\log L}$. In More et al. (2011), where they derive constraints for both $\sigma_{\log L}$ and $\sigma_{\log M_*}$ from the same data, they find $\sigma_{\log M_*} = 0.15^{+0.08}_{-0.11} < \sigma_{\log L} = 0.21^{+0.06}_{-0.04}$ for blue centrals. However, translating from $\sigma_{\log L}$ to $\sigma_{\log M_*}$ is difficult for an analysis that uses different data set and model. Overlooking the varoius caveats of the analyses, $\sigma_{\log M_*}$ from Cao et al. (in preparation) is in tension with the other constraints. **CH:** @JLT: sentence on the Cao et al. discrepancy?. We also note that these observational constraints include significant measurement uncertainties in M_*. The intrinsic $\sigma_{\log M_*}$ of these constraints, which is the scatter predicted by our model, will thus be reduced. For example, if we consider $0.1 - 0.2$ dex uncertainties in M_* (Roediger & Courteau 2015), the Cao et al. (in preparation) constraint will be reduced from $\sigma_{\log M_*} = 0.33$ dex to $0.31 - 0.26$ dex. Hence, despite the tension, observational constraints overall favor a shorter duty cycle timescale.

In addition to the observational constraints, we also compare the $\sigma_{\log M_*}(M_h \sim 10^{12} M_\odot)$ predicted by our model to predictions from modern galaxy formation models on the right panel: hydrodynamic simulations (dot filled), semi-analytic models (SAM; hatched), and an empirical model (dashed line). For the hydrodynamic simulations, the dotted region, $\sigma_{\log M_*} = 0.16 - 0.22$ dex, encompasses pre-

dictions from EAGLE (McAlpine et al. 2016), Massive Black II (Khandai et al. 2015), and Illustris TNG (Pillepich et al. 2018), as compiled in Figure 8 of Wechsler & Tinker (2018). For the SAMs, the hatched region, $\sigma_{\log M_*} = 0.3 - 0.37$ dex, includes predictions from Lu et al. (2014); Somerville et al. (2012), and the SAGE model[2]. We also include the prediction from the empirical model in Behroozi et al. (2018) (UniverseMachine). $\sigma_{\log M_*}$ from SAMs are consistent with our model with $t_{\rm duty} \gtrsim 5$ Gyr. The UniverseMachine, which predicts a lower $\sigma_{\log M_*}$, is consistent with $t_{\rm duty} = 1 - 5$ Gyr. Lastly, hydrodynamic simulations predict the lowest $\sigma_{\log M_*}$ among the models ~ 0.2 dex, which cannot be reproduced by our model even with the shortest $t_{\rm duty}$ timescale that we consider.

Although there is no clear consensus among the observational $\sigma_{\log M_*}$ constraints at $M_h \sim 10^{12} M_\odot$ (Figure 5 left panel), at $M_h > 10^{12} M_\odot$ observations are in better agreement and *only* hydrodynamic simulations predict $\sigma_{\log M_*}$ low enough to be consistent (Wechsler & Tinker 2018). Thus, focusing the comparison to observational constraints and predictions from hydrodynamic simulations, we conclude that SF central galaxies have star formation varability on short timescales, $\lesssim 1$ Gyr. In fact, star formation variability in the SFH alone may be insufficient to produce the tight scatter in SHMR found in observations and hydrodynamic simulations.

4.2. *The Need for Assembly Bias?*

A shorter star formation duty cycle timescale produces smaller scatter in the SHMR of our model. This dependence on the duty cycle timescale, allows us to compare our model with measurements of $\sigma_{\log M_*}$ and predictions from galaxy formation models to constrain $t_{\rm duty}$, which reflect the star formation variability timescale. Such comparisons in the previous section, demonstrate that $t_{\rm duty} \lesssim 1\,$Gyr is favored by observational constraints. Meanwhile a short duty cycle timescale alone is not enough to conservatively reproduce the $\sigma_{\log M_*}$ constraints predicted by hydrodynamic simulations. In our fiducial model, the SFR and M_* evolution of star-forming centrals are independent from the host halo properties. There is, however, growing evidence that star formation in galaxies correlate with their host halo accretion histories (*e.g.* Lim et al. 2016; Tojeiro et al. 2017; Tinker et al. 2018a). Therefore, in this section, we introduce *assembly bias* into the SFH prescription of our model and investigate its impact on $\sigma_{\log M_*}$.

Assembly bias, most commonly in the literature, refers to the dependence of the spatial distribution of dark matter halos on halo properties besides mass (Gao et al. 2005; Wechsler et al. 2006; Gao & White 2007; Wetzel et al. 2007; Li et al. 2008; Sunayama et al. 2016). At low halo mass, older and more concentrated halos form in high density environments. While at high halo mass, the effect is the opposite — younger, less concentrated halos form in high-density regions. However, both simulations (*e.g.* Croton et al. 2007; Artale et al. 2018; Zehavi et al. 2018) as well as observations (Yang et al. 2006; Wang et al. 2008; Tinker et al. 2011; Wang et al. 2013; Lacerna et al. 2014; Tinker et al. 2018b), find that this assembly bias propagates beyond spatial clustering and correlates with various galaxy properties such as formation histories and star formation properties, an effect more specifically referred to as *galaxy* assembly bias. In our model, we incorporate galaxy assembly bias by correlating

[2] https://tao.asvo.org.au/tao/

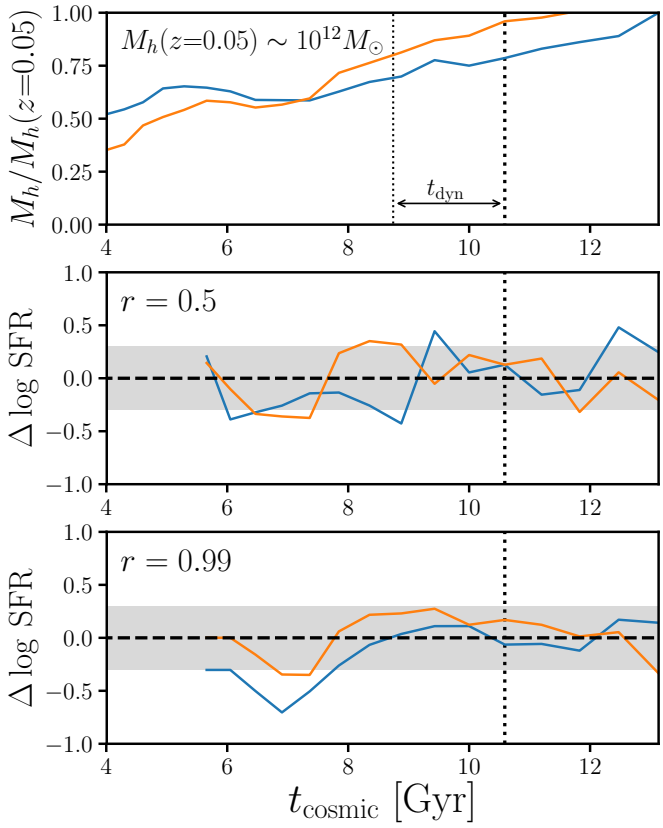

Figure 6. We incorporate assembly bias into the SF centrals of our model by correlating their host halo accretion history with their SFH with respect to the SFS. We plot the relative halo accretion history, $M_h(t)/M_h(z{=}0.05)$ for two randomly chosen SF centrals with $M_h(z{=}0.05) \sim 10^{12} M_\odot$, in the top panel. In the two panels below we present $\Delta \log$ SFR, SFH with respect to the SFS, of these galaxies for our model with correlation coefficients $r = 0.5$ and 0.99 (middle and bottom). The shaded region in these panels mark the 0.3 dex 1-sigma width of the SFS. At some t (dotted), $\Delta \log \mathrm{SFR}(t)$ is correlated with halo accretion over the period $t - t_{\rm dyn}$ to $t_{\rm dyn}$ labeled in top panel. The SFHs illustrate how $\Delta \log \mathrm{SFR}(t)$ correlates with $\Delta M_h = M_h(t) - M_h(t - t_{\rm dyn})$ and how $\Delta \log \mathrm{SFR}(t)$ correlates more strongly with $\Delta M_h(t)$ with higher r.

the SFHs of our star-forming central galaxies and their host halo accretion histories with a correlation coefficient r.

Motivated by the correlation between in log SSFR and halo accretion rate found in Tinker et al. (2018b), we correlate a galaxy's SFR with respect to the mean SFS SFR (*i.e.* $\Delta \log$ SFR in Eq. 3) to the halo mass accretion over dynamical time. At every $t_{\rm duty}$ timestep, t, $\Delta \log \mathrm{SFR}(t)$ is assigned based on $\Delta M_h(t) = M_h(t) - M_h(t - t_{\rm dyn}(t))$ in $M_{\rm max}$ bins with a correlation coefficient r, a parameter added to our model. As we mention earlier, this prescription for correlating $\Delta \log$ SFR to ΔM_h is similar to other empirical models that also correlate $\Delta \log$ SFR to ΔM_h over $t_{\rm dyn}$ (Watson et al. 2015; Rodríguez-Puebla et al. 2016; Behroozi et al. 2018). In their prescriptions of $\Delta \log$ SFR, however, these models do not focus on a specific timescale of star formation variability as our model does through the star formation duty cycle.

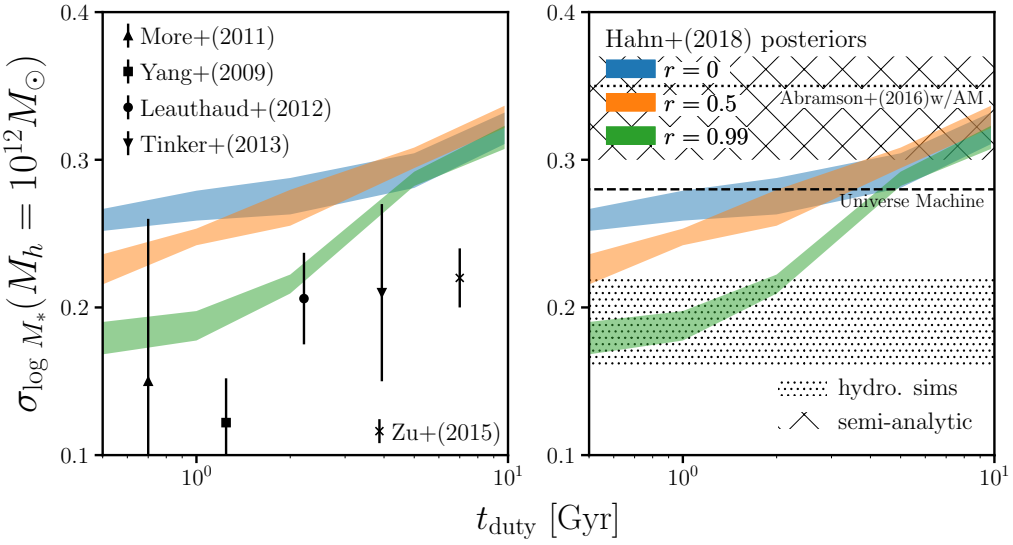

Figure 7. When we incorporate assembly bias, $\sigma_{\log M_*}$ of our model spans the various observational constraints and predictions from galaxy formation models. We plot $\sigma_{\log M_*}(M_h = 10^{12} M_\odot)$ as a function of the star formation duty cycle timescale, $t_{\rm duty}$, for our best-fit model with no assembly bias (blue) and with correlation coefficients between host halo accretion history and SFH of r=0.5 (orange) and 0.99 (green). Stronger assembly bias at $t_{\rm duty}$<5 Gyr significantly reduces the scatter in SHMR, $\sigma_{\log M_*}$. In the left panel, we include observational cosntraints from Figure 5; in the right, we include predictions from hydrodyanmical simulations (dotted region), semi-analytic models (hatched), and the UniverseMachine (Behroozi et al. 2018) (dashed). We also include on the right $\sigma_{\log M_*}$ derived from matching Abramson et al. (2016) SFHs to halos via abundance matching. With strong assembly bias and $t_{\rm duty} < 1$ Gyr, our model conservatively agrees with $\sigma_{\log M_*}$ observational cosntraints and predictions from hydrodynamic simulations.

In Figure 6 we illustrate this prescription for galaxy assembly bias in our model. We plot the relative halo accretion histories $M_h(t)/M_h(z{=}0.05)$ of two arbitrarily chosen SF centrals with $M_h(z{=}0.05) \sim 10^{12} M_\odot$ in the top panel (orange and blue). Below, we plot $\Delta \log {\rm SFR}$, SFH with respect to the SFS, of these galaxies for our model with correlation coefficients $r = 0.5$ and 0.99 (middle and bottom). At some t, we choose a random `TreePM` snapshot (dotted), and label the period $[t, t - t_{\rm dyn}]$. Halo accretion over this period, $\Delta M_h = M_h(t) - M_h(t - t_{\rm dyn})$, correlates with $\Delta \log {\rm SFR}(t)$. The SFHs in the middle and bottom panels illustrate this correlation and how $\Delta \log {\rm SFR}(t)$ correlates more strongly with $\Delta M_h(t)$ for our model with higher r.

We then repeat our analysis of inferring model parameters by comparing to observations using ABC-PMC — this time for our model with galaxy assembly bias over a grid of $t_{\rm duty}$ and r values. Using the resulting posterior distributions, we examine the scatter in the SHMR ($\sigma_{\log M_*}$) predicted by our model as a function of $t_{\rm duty}$ with $r = 0$ (no assembly bias; blue), 0.5 (orange), and 0.99 (green) in Figure 7. The shaded regions represent the 68% confidence interval of the predicted $\sigma_{\log M_*}$. We again emphasize that for all sets of ($t_{\rm duty}$, r) our models reproduce the observed SMF of SF centrals and SFS. At $t_{\rm duty} \geq 5$ Gyr we find no significant difference in $\sigma_{\log M_*}$, regardless of r. Below $t_{\rm duty} < 5$ Gyr, however, $\sigma_{\log M_*}$ of our model decreases significantly as the SFH of SF galaxies are more correlated

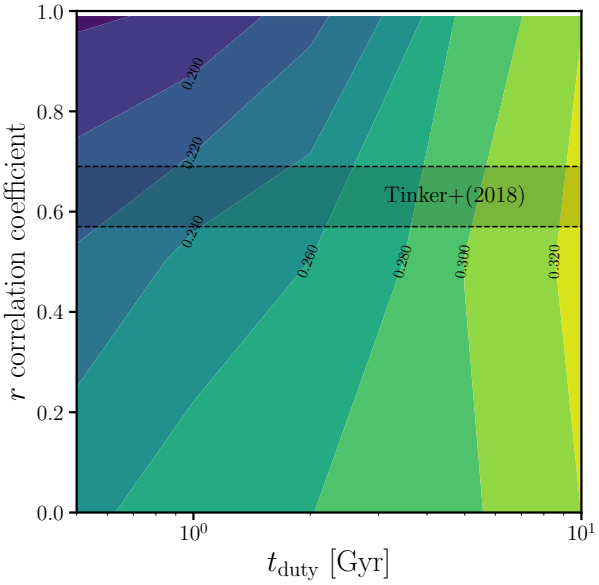

Figure 8.

with halo accretion history. For $t_{\rm duty} = 0.5\,{\rm Gyr}$, we find $\sigma_{\log M_*} = 0.26^{+0.010}_{-0.012}, 0.22^{+0.013}_{-0.005}$, and $0.17^{+0.007}_{-0.015}$ for $r = 0.0, 0.5$, and 0.99, respectively.

Comparing our updated model to the observational constraints included in Figure 5, we find that incorporating assembly bias significantly reduces the tensions with the More et al. (2011); Leauthaud et al. (2012); Reddick et al. (2013); Tinker et al. (2013); Zu & Mandelbaum (2015) constraints (left panel of Figure 7). In fact, with a short star formation duty cycle ($t_{\rm duty} \leq 1\,{\rm Gyr}$) and galaxy assembly bias with $r \geq 0.5$, our model is in agreement with these $\sigma_{\log M_*} \sim 0.2$ dex constraints. On the other hand, for our model with shorter $t_{\rm duty} < 2$ Gyr, assembly bias increases the tension with the Cao et al. (in preparation) constraint. In addition to the observations, on the right panel, we compare our updated model to predictions from galaxy formation models included in Figure 5. By varying r and $t_{\rm duty}$, $\sigma_{\log M_*}$ of our model can reproduce all of the model predictions. Focusing again on hydrodynamic simulations, which are the only models that reproduce the high M_h $\sigma_{\log M_*}$ constraints, we find that galaxy assembly bias improves the tension with our model. With a short duty cycle timescale, $t_{\rm duty} < 1$ Gyr and $r > 0.5$, our model produces the tight scatter in SHMR found in hydrodynamic simulations.

The $\sigma_{\log M_*}$ in Figure 7 also reveal degeneracy between $t_{\rm duty}$ and r. A shorter $t_{\rm duty}$ or higher r can produce smaller $\sigma_{\log M_*}$. We further illustrate this degeneracy in Figure 8, where we plot $\sigma_{\log M_*}$ (contour and color map) as a function of $t_{\rm duty}$ and r. Regardless of the degeneracy, to produce $\sigma_{\log M_*} \sim 0.2$ dex, as found in some observations and predicted by hydrodynamic simulations, both $t_{\rm duty} \leq 1$ Gyr and $r > 0.5$. **CH:** there are some constraints on r from the literature

A key element of our model is the SFH prescription for SF central galaxies where the SFH evolves about the SFS. Contrary to our SFH prescription, Kelson (2014), for example, argue that the SFS is a simple consequence of central limit theorem and can be reproduced even if *in situ* stellar mass

growth is modeled as a stochastic process like a random walk. Gladders et al. (2013); Abramson et al. (2015, 2016), similarly argue that ~ 2000 loosely constrained log-normal SFHs can reproduce observations such as the SMF at $z \leq 8$ and the SFS at $z \leq 6$. These works, however, focus on reproducing observations of galaxy properties and do not examine the galaxy-halo connection such as the SHMR. In order to test whether log-normal SFHs can also produce realistic SHMRs, we take the SFHs, SFR(t) and $M_*(t)$, from Abramson et al. (2016) and assign them to halos by abundance matching their M_* to M_h at $z{\sim}1$. We then restrict the SFHs to those that would be classified as star-forming based on a rough log SSFR $> -11.$ cut. Afterwards we measure $\sigma_{\log M_*}$ at the lowest M_h where it can be reliably measured given the Abramson et al. (2016) sample's $M_*{>}10^{10} M_\odot$ limit. Based o our abundance matching prescription, we find Abramson et al. (2016) predicts a scatter of $\sigma_{\log M_*}(M_h = 10^{12.4}) = 0.33 \pm 0.04$ (dotted line in Figure 7). Despite the Abramson et al. (2016) SFHs can reproduce a number of galaxy observations, $\sigma_{\log M_*}$ derived from the SFHs and abundance matching predict SHMR scatters too high compared to constraints from observations and predictions from hydrodynamic simulations. This estimate is, however, derived from a simple abundance matching scheme. As Diemer et al. (2017) find from their log-normal fits to the SFHs of Illustris galaxies, halo formation history correlates with the fits. Incorporating such assembly bias into our abundance matching may reduce $\sigma_{\log M_*}$.

In this section, we demonstrate that incorporating assembly bias into our model by correlating $\Delta \log \mathrm{SFR}$ to ΔM_h reduces the tension with the SHMR scatter in observations. With assembly bias added, our model can produce the range of $\sigma_{\log M_*}$ constraints from observations as well as modern galaxy formation models. However, even with assembly bias a short duty cycle is *necessary* to produce tight scatter in the SHMR. This further confirms our conclusion from the previous section that the SFRs of star-forming central galaxies have variations on $\lesssim 0.5$ Gyr timescales. Furthermore, with a short star formation duty cycle timescale and strong assembly bias $r > 0.5$, our model conservatively agrees with observational constraints and produces tight scatter in the SHMR, unlike predictions from semi-analytic models and UniverseMachine. Our comparison not only provides constraints on the timescale of star formation variability, but it also confirms the role of assembly bias in the SFH of star-forming galaxies.

5. SUMMARY AND CONCLUSION

some brief intro paragraph consistent with the intro

We combine the high-resolution cosmological N-body `TreePM` simulation with SFHs that evolve the SF central galaxies along the SFS and present a model that tracks the SFR, M_*, and host halo accretion histories of SF centrals from $z \sim 1$ to $z = 0.05$. More specifically, we characterize the SFHs to evolve with respect to the mean log SFR of the SFS with a "star formation duty cycle" that introduces variability on some specific timescale, $t_{\rm duty}$. Besides $t_{\rm duty}$, we parameterize the SFS using **parameters**, free parameters that dictate the low M_* and high M_* slopes and redshift evolution. With priors for these parameters set to only produce SFS within observed range, we use ABC-PMC to infer a model that reproduce the observed SMF of the SF centrals in the SDSS DR7 group catalog. When we examine the SHMR of this model we find:

- A shorter star formation duty cycle in our model produces significantly tighter scatter in the SHMR both for fixed $M_h = 10^{12} M_\odot$ and $M_* = 10^{10} M_\odot$. As $t_{\rm duty}$ ranges from 10 to 0.5 Gyr, $\sigma_{\log M_*} = 0.32^{+0.019}_{-0.021}$ to $0.26^{+0.010}_{-0.012}$ and $\sigma_{\log M_h} = 0.30^{+0.005}_{-0.006}$ to $0.19^{+0.008}_{-0.006}$. The dependence of $\sigma_{\log M_*}$ and $\sigma_{\log M_h}$ on $t_{\rm duty}$ demonstrates that the scatter in SHMR provides some constraint on $t_{\rm duty}$ and the timescale of star formation variability.

- We compare the $\sigma_{\log M_*}$ and $\sigma_{\log M_h}$ predicted by our model to constraints from halo occupation modeling of galaxy clustering, SMF, satellite kinematics, and galaxy-galaxy weak lensing observations. The $\sigma_{\log M_h}$ comparison does not significantly constrain $t_{\rm duty}$. However, from the $\sigma_{\log M_*}$ comparison, we find that a duty cycle with $t_{\rm duty} \lesssim 0.5$ Gyr is necessary to reduce the tension with observations.

- We next incorporate assembly bias into our model by allowing the star formation histories to correlate with halo accretion histories by a correlation coefficient, r. With assembly bias, our model can predict $\sigma_{\log M_*}$=0.17 to 0.33, which spans the predictions from modern galaxy formation models. However, to conservatively reproduce $\sigma_{\log M_*}$ predictions from hydrodynamic simulations and constraints from observations, a short duty cycle and $r > 0.5$— *i.e.* strong assembly bias— is required.

Paragraph about implications of our results
Paragraph about future with DESI BGS.

ACKNOWLEDGEMENTS

It's a pleasure to thank J.D. Cohn, Shirley Ho, and Tjitske Starkenburg for valuable discussions and feedback. We also thank Louis E. Abramson, Junzhi Cao, Shy Genel, and Cheng Li for providing us with data used in the analysis. This material is based upon work supported by the U.S. Department of Energy, Office of Science, Office of High Energy Physics, under contract No. DE-AC02-05CH11231.

REFERENCES

Abazajian, K. N., Adelman-McCarthy, J. K., Agüeros, M. A., et al. 2009, The Astrophysical Journal Supplement Series, 182, 543, doi: 10.1088/0067-0049/182/2/543

Abramson, L. E., Gladders, M. D., Dressler, A., et al. 2016, The Astrophysical Journal, 832, 7, doi: 10.3847/0004-637X/832/1/7

—. 2015, The Astrophysical Journal Letters, 801, L12, doi: 10.1088/2041-8205/801/1/L12

Alsing, J., Wandelt, B., & Feeney, S. 2018, arXiv:1801.01497 [astro-ph]. https://arxiv.org/abs/1801.01497

Artale, M. C., Zehavi, I., Contreras, S., & Norberg, P. 2018, Monthly Notices of the Royal Astronomical Society, 480, 3978, doi: 10.1093/mnras/sty2110

Baldry, I. K., Balogh, M. L., Bower, R. G., et al. 2006, Monthly Notices of the Royal Astronomical Society, 373, 469, doi: 10.1111/j.1365-2966.2006.11081.x

Behroozi, P., Wechsler, R., Hearin, A., & Conroy, C. 2018, ArXiv e-prints, 1806, arXiv:1806.07893

Blanton, M. R., & Moustakas, J. 2009, Annual Review of Astronomy and Astrophysics, 47, 159, doi: 10.1146/annurev-astro-082708-101734

Blanton, M. R., & Roweis, S. 2007, The Astronomical Journal, 133, 734, doi: 10.1086/510127

Blanton, M. R., Schlegel, D. J., Strauss, M. A., et al. 2005, The Astronomical Journal, 129, 2562, doi: 10.1086/429803

Brinchmann, J., Charlot, S., White, S. D. M., et al. 2004, Monthly Notices of the Royal Astronomical Society, 351, 1151, doi: 10.1111/j.1365-2966.2004.07881.x

Cameron, E., & Pettitt, A. N. 2012, Monthly Notices of the Royal Astronomical Society, 425, 44, doi: 10.1111/j.1365-2966.2012.21371.x

Campbell, D., van den Bosch, F. C., Hearin, A., et al. 2015, Monthly Notices of the Royal Astronomical Society, 452, 444, doi: 10.1093/mnras/stv1091

Carnall, A. C., Leja, J., Johnson, B. D., et al. 2018, arXiv:1811.03635 [astro-ph]. https://arxiv.org/abs/1811.03635

Chabrier, G. 2003, Publications of the Astronomical Society of the Pacific, 115, 763, doi: 10.1086/376392

Coil, A. L., Blanton, M. R., Burles, S. M., et al. 2011, The Astrophysical Journal, 741, 8, doi: 10.1088/0004-637X/741/1/8

Conroy, C., Wechsler, R. H., & Kravtsov, A. V. 2006, The Astrophysical Journal, 647, 201, doi: 10.1086/503602

Conroy, C., Prada, F., Newman, J. A., et al. 2007, The Astrophysical Journal, 654, 153, doi: 10.1086/509632

Cool, R. J., Moustakas, J., Blanton, M. R., et al. 2013, The Astrophysical Journal, 767, 118, doi: 10.1088/0004-637X/767/2/118

Croton, D. J., Gao, L., & White, S. D. M. 2007, Monthly Notices of the Royal Astronomical Society, 374, 1303, doi: 10.1111/j.1365-2966.2006.11230.x

Daddi, E., Dickinson, M., Morrison, G., et al. 2007, The Astrophysical Journal, 670, 156, doi: 10.1086/521818

Davis, M., Efstathiou, G., Frenk, C. S., & White, S. D. M. 1985, The Astrophysical Journal, 292, 371, doi: 10.1086/163168

Diemer, B., Sparre, M., Abramson, L. E., & Torrey, P. 2017, The Astrophysical Journal, 839, 26, doi: 10.3847/1538-4357/aa68e5

Drory, N., Bundy, K., Leauthaud, A., et al. 2009, The Astrophysical Journal, 707, 1595, doi: 10.1088/0004-637X/707/2/1595

Elbaz, D., Daddi, E., Le Borgne, D., et al. 2007, Astronomy and Astrophysics, 468, 33, doi: 10.1051/0004-6361:20077525

Gao, L., Springel, V., & White, S. D. M. 2005, Monthly Notices of the Royal Astronomical Society, 363, L66, doi: 10.1111/j.1745-3933.2005.00084.x

Gao, L., & White, S. D. M. 2007, Monthly Notices of the Royal Astronomical Society, 377, L5, doi: 10.1111/j.1745-3933.2007.00292.x

Genel, S., Vogelsberger, M., Springel, V., et al. 2014, Monthly Notices of the Royal Astronomical Society, 445, 175, doi: 10.1093/mnras/stu1654

Gladders, M. D., Oemler, A., Dressler, A., et al. 2013, The Astrophysical Journal, 770, 64, doi: 10.1088/0004-637X/770/1/64

Gu, M., Conroy, C., & Behroozi, P. 2016, The Astrophysical Journal, 833, 2, doi: 10.3847/0004-637X/833/1/2

Hahn, C., Tinker, J. L., & Wetzel, A. R. 2017a, The Astrophysical Journal, 841, 6, doi: 10.3847/1538-4357/aa6d6b

Hahn, C., Vakili, M., Walsh, K., et al. 2017b, Monthly Notices of the Royal Astronomical Society, 469, 2791, doi: 10.1093/mnras/stx894

Hahn, C., Blanton, M. R., Moustakas, J., et al. 2015, The Astrophysical Journal, 806, 162, doi: 10.1088/0004-637X/806/2/162

Hahn, C., Starkenburg, T. K., Choi, E., et al. 2018

Han, J., Eke, V. R., Frenk, C. S., et al. 2015, Monthly Notices of the Royal Astronomical Society, 446, 1356, doi: 10.1093/mnras/stu2178

Ilbert, O., McCracken, H. J., Le Fèvre, O., et al. 2013, Astronomy and Astrophysics, 556, A55, doi: 10.1051/0004-6361/201321100

Ishida, E. E. O., Vitenti, S. D. P., Penna-Lima, M., et al. 2015, Astronomy and Computing, 13, 1, doi: 10.1016/j.ascom.2015.09.001

Karim, A., Schinnerer, E., Martínez-Sansigre, A., et al. 2011, The Astrophysical Journal, 730, 61, doi: 10.1088/0004-637X/730/2/61

Kelson, D. D. 2014, arXiv:1406.5191 [astro-ph]. https://arxiv.org/abs/1406.5191

Khandai, N., Di Matteo, T., Croft, R., et al. 2015, Monthly Notices of the Royal Astronomical Society, 450, 1349, doi: 10.1093/mnras/stv627

Lacerna, I., Padilla, N., & Stasyszyn, F. 2014, Monthly Notices of the Royal Astronomical Society, 443, 3107, doi: 10.1093/mnras/stu1318
Lange, J. U., van den Bosch, F. C., Zentner, A. R., Wang, K., & Villarreal, A. S. 2018, arXiv:1811.03596 [astro-ph]. https://arxiv.org/abs/1811.03596
Leauthaud, A., Tinker, J., Bundy, K., et al. 2012, The Astrophysical Journal, 744, 159, doi: 10.1088/0004-637X/744/2/159
Lee, N., Sanders, D. B., Casey, C. M., et al. 2015, The Astrophysical Journal, 801, 80, doi: 10.1088/0004-637X/801/2/80
Leja, J., Carnall, A. C., Johnson, B. D., Conroy, C., & Speagle, J. S. 2018, arXiv:1811.03637 [astro-ph]. https://arxiv.org/abs/1811.03637
Leja, J., van Dokkum, P., & Franx, M. 2013, The Astrophysical Journal, 766, doi: 10.1088/0004-637X/766/1/33
Li, C., & White, S. D. M. 2009, Monthly Notices of the Royal Astronomical Society, 398, 2177, doi: 10.1111/j.1365-2966.2009.15268.x
Li, Y., Mo, H. J., & Gao, L. 2008, Monthly Notices of the Royal Astronomical Society, 389, 1419, doi: 10.1111/j.1365-2966.2008.13667.x
Lim, S. H., Mo, H. J., Wang, H., & Yang, X. 2016, Monthly Notices of the Royal Astronomical Society, 455, 499, doi: 10.1093/mnras/stv2282
Lu, Y., Wechsler, R. H., Somerville, R. S., et al. 2014, The Astrophysical Journal, 795, 123, doi: 10.1088/0004-637X/795/2/123
Magdis, G. E., Daddi, E., Béthermin, M., et al. 2012, The Astrophysical Journal, 760, 6, doi: 10.1088/0004-637X/760/1/6
Mamon, G. A., Sanchis, T., Salvador-Solé, E., & Solanes, J. M. 2004, Astronomy and Astrophysics, 414, 445, doi: 10.1051/0004-6361:20034155
Mandelbaum, R., Seljak, U., Kauffmann, G., Hirata, C. M., & Brinkmann, J. 2006, Monthly Notices of the Royal Astronomical Society, 368, 715, doi: 10.1111/j.1365-2966.2006.10156.x
Marchesini, D., van Dokkum, P. G., Förster Schreiber, N. M., et al. 2009, The Astrophysical Journal, 701, 1765, doi: 10.1088/0004-637X/701/2/1765
McAlpine, S., Helly, J. C., Schaller, M., et al. 2016, Astronomy and Computing, 15, 72, doi: 10.1016/j.ascom.2016.02.004
Mitra, S., Davé, R., & Finlator, K. 2015, Monthly Notices of the Royal Astronomical Society, 452, 1184, doi: 10.1093/mnras/stv1387
More, S., van den Bosch, F. C., Cacciato, M., et al. 2011, Monthly Notices of the Royal Astronomical Society, 410, 210, doi: 10.1111/j.1365-2966.2010.17436.x
Moustakas, J., Coil, A. L., Aird, J., et al. 2013, The Astrophysical Journal, 767, 50, doi: 10.1088/0004-637X/767/1/50
Muzzin, A., Marchesini, D., Stefanon, M., et al. 2013, The Astrophysical Journal, 777, 18, doi: 10.1088/0004-637X/777/1/18
Noeske, K. G., Weiner, B. J., Faber, S. M., et al. 2007, The Astrophysical Journal Letters, 660, L43, doi: 10.1086/517926
Peng, Y.-j., Lilly, S. J., Kovač, K., et al. 2010, The Astrophysical Journal, 721, 193, doi: 10.1088/0004-637X/721/1/193
Pillepich, A., Springel, V., Nelson, D., et al. 2018, Monthly Notices of the Royal Astronomical Society, 473, 4077, doi: 10.1093/mnras/stx2656
Reddick, R. M., Wechsler, R. H., Tinker, J. L., & Behroozi, P. S. 2013, The Astrophysical Journal, 771, 30, doi: 10.1088/0004-637X/771/1/30
Rodríguez-Puebla, A., Primack, J. R., Behroozi, P., & Faber, S. M. 2016, Monthly Notices of the Royal Astronomical Society, 455, 2592, doi: 10.1093/mnras/stv2513
Roediger, J. C., & Courteau, S. 2015, Monthly Notices of the Royal Astronomical Society, 452, 3209, doi: 10.1093/mnras/stv1499
Salim, S., Rich, R. M., Charlot, S., et al. 2007, The Astrophysical Journal Supplement Series, 173, 267, doi: 10.1086/519218
Santini, P., Fontana, A., Grazian, A., et al. 2009, Astronomy and Astrophysics, 504, 751, doi: 10.1051/0004-6361/200811434
Scoville, N., Aussel, H., Brusa, M., et al. 2007, The Astrophysical Journal Supplement Series, 172, 1, doi: 10.1086/516585
Somerville, R. S., & Davé, R. 2015, Annual Review of Astronomy and Astrophysics, 53, 51, doi: 10.1146/annurev-astro-082812-140951
Somerville, R. S., Gilmore, R. C., Primack, J. R., & Domínguez, A. 2012, Monthly Notices of the Royal Astronomical Society, 423, 1992, doi: 10.1111/j.1365-2966.2012.20490.x

Speagle, J. S., Steinhardt, C. L., Capak, P. L., & Silverman, J. D. 2014, The Astrophysical Journal Supplement Series, 214, 15, doi: 10.1088/0067-0049/214/2/15

Sunayama, T., Hearin, A. P., Padmanabhan, N., & Leauthaud, A. 2016, Monthly Notices of the Royal Astronomical Society, 458, 1510, doi: 10.1093/mnras/stw332

Tinker, J., Wetzel, A., & Conroy, C. 2011, ArXiv e-prints, 1107, arXiv:1107.5046

Tinker, J. L., Hahn, C., Mao, Y.-Y., & Wetzel, A. R. 2018a, Monthly Notices of the Royal Astronomical Society, 478, 4487, doi: 10.1093/mnras/sty1263

Tinker, J. L., Hahn, C., Mao, Y.-Y., Wetzel, A. R., & Conroy, C. 2018b, Monthly Notices of the Royal Astronomical Society, 477, 935, doi: 10.1093/mnras/sty666

Tinker, J. L., Leauthaud, A., Bundy, K., et al. 2013, The Astrophysical Journal, 778, 93, doi: 10.1088/0004-637X/778/2/93

Tinker, J. L., Wetzel, A. R., Conroy, C., & Mao, Y.-Y. 2017, Monthly Notices of the Royal Astronomical Society, 472, 2504, doi: 10.1093/mnras/stx2066

Tojeiro, R., Wilkins, S., Heavens, A. F., Panter, B., & Jimenez, R. 2009, The Astrophysical Journal Supplement Series, 185, 1, doi: 10.1088/0067-0049/185/1/1

Tojeiro, R., Eardley, E., Peacock, J. A., et al. 2017, Monthly Notices of the Royal Astronomical Society, 470, 3720, doi: 10.1093/mnras/stx1466

Vale, A., & Ostriker, J. P. 2006, Monthly Notices of the Royal Astronomical Society, 371, 1173, doi: 10.1111/j.1365-2966.2006.10605.x

Velander, M., van Uitert, E., Hoekstra, H., et al. 2014, Monthly Notices of the Royal Astronomical Society, 437, 2111, doi: 10.1093/mnras/stt2013

Vogelsberger, M., Genel, S., Springel, V., et al. 2014, Monthly Notices of the Royal Astronomical Society, 444, 1518, doi: 10.1093/mnras/stu1536

Wang, L., Farrah, D., Oliver, S. J., et al. 2013, Monthly Notices of the Royal Astronomical Society, 431, 648, doi: 10.1093/mnras/stt190

Wang, Y., Yang, X., Mo, H. J., et al. 2008, The Astrophysical Journal, 687, 919, doi: 10.1086/591836

Watson, D. F., Hearin, A. P., Berlind, A. A., et al. 2015, Monthly Notices of the Royal Astronomical Society, 446, 651, doi: 10.1093/mnras/stu2065

Wechsler, R. H., & Tinker, J. L. 2018, ArXiv e-prints, 1804, arXiv:1804.03097

Wechsler, R. H., Zentner, A. R., Bullock, J. S., Kravtsov, A. V., & Allgood, B. 2006, The Astrophysical Journal, 652, 71, doi: 10.1086/507120

Wetzel, A. R., Cohn, J. D., & White, M. 2009, Monthly Notices of the Royal Astronomical Society, 395, 1376, doi: 10.1111/j.1365-2966.2009.14424.x

Wetzel, A. R., Cohn, J. D., White, M., Holz, D. E., & Warren, M. S. 2007, The Astrophysical Journal, 656, 139, doi: 10.1086/510444

Wetzel, A. R., Tinker, J. L., & Conroy, C. 2012, Monthly Notices of the Royal Astronomical Society, 424, 232, doi: 10.1111/j.1365-2966.2012.21188.x

Wetzel, A. R., Tinker, J. L., Conroy, C., & van den Bosch, F. C. 2013, Monthly Notices of the Royal Astronomical Society, 432, 336, doi: 10.1093/mnras/stt469

—. 2014, Monthly Notices of the Royal Astronomical Society, 439, 2687, doi: 10.1093/mnras/stu122

Wetzel, A. R., & White, M. 2010, Monthly Notices of the Royal Astronomical Society, 403, 1072, doi: 10.1111/j.1365-2966.2009.16191.x

Weyant, A., Schafer, C., & Wood-Vasey, W. M. 2013, The Astrophysical Journal, 764, 116, doi: 10.1088/0004-637X/764/2/116

Whitaker, K. E., van Dokkum, P. G., Brammer, G., & Franx, M. 2012, The Astrophysical Journal Letters, 754, L29, doi: 10.1088/2041-8205/754/2/L29

White, M. 2002, The Astrophysical Journal Supplement Series, 143, 241, doi: 10.1086/342752

White, M., Cohn, J. D., & Smit, R. 2010, Monthly Notices of the Royal Astronomical Society, 408, 1818, doi: 10.1111/j.1365-2966.2010.17248.x

Wilkinson, D. M., Maraston, C., Goddard, D., Thomas, D., & Parikh, T. 2017, arXiv:1711.00865 [astro-ph]. https://arxiv.org/abs/1711.00865

Yang, X., Mo, H. J., & van den Bosch, F. C. 2006, The Astrophysical Journal Letters, 638, L55, doi: 10.1086/501069

—. 2009, The Astrophysical Journal, 695, 900, doi: 10.1088/0004-637X/695/2/900

Zehavi, I., Contreras, S., Padilla, N., et al. 2018, The Astrophysical Journal, 853, 84, doi: 10.3847/1538-4357/aaa54a

Zu, Y., & Mandelbaum, R. 2015, Monthly Notices of the Royal Astronomical Society, 454, 1161, doi: 10.1093/mnras/stv2062